Int. J. Heat Mass Transfer. Vol. 34, No. 7, pp. 1847–1859, 1991
Printed in Great Britain

0017–9310/91 $3.00 + 0.00

Holographic interferometry experiments on the growth of ice from a horizontal pipe

T. L. SPATZ and D. POULIKAKOS
Mechanical Engineering Department, University of Illinois at Chicago, P.O. Box 4348, Chicago, IL 60680, U.S.A.

(*Received* 30 *March* 1990 *and in final form* 17 *September* 1990)

Abstract—In this paper the main results of an experimental study on the growth of ice from an internally cooled horizontal pipe immersed in water are reported. With the help of holographic interferometry, the local Nusselt number at the solidifying interface is obtained at characteristic times during the evolution of the solidification phenomenon. Visualization proved that the temperature and flow fields at the early stages of the solidification are nonsymmetric and unstable. A buoyancy-driven plume develops on the underside of the pipe and flows downward. This plume swings continuously about the vertical axis of symmetry of the system and affects the solidification process. Additional key results reported in this paper include the evolution of the phase change interface with time, the dependence of the pipe wall temperature on time and the dependence of the volume of ice produced on time.

1. INTRODUCTION

FREEZING of water around pipes occurs in many thermal engineering applications that use water as the working fluid. These applications are exemplified by heat exchangers of various types, thermal storage systems and ice production systems. It is of importance, then, to understand the fundamentals as well as to produce reliable quantitative information for the phenomenon of ice growth around an internally cooled pipe immersed in water. In the following paragraphs, key results published in the open literature related directly or indirectly to the above-mentioned problem will be discussed.

Reimann [1] investigated experimentally the free convection flow from isothermal wires in the vicinity of impermeable boundaries. These boundaries were a solid wall or the surface of a liquid. The wire approached the interface from above or below. It was found that the total heat transfer generated by the wire does not vary monotonically with the distance of the wire from the boundary. Even though the problem in ref. [1] is not directly related to the present investigation, it contains interesting photographs of visualization of the temperature field obtained using Mach–Zehnder interferometry. Holographic visualization of natural convection from a horizontal hot wire to a liquid illustrating the effect of transverse oscillations on heat transfer was reported by Antonini *et al.* [2].

Solidification of paraffin around a cooled horizontal cylinder was explored by Bathelt *et al.* [3]. The results obtained show that the effects of natural convection at the phase change boundary must be accounted for, in order to obtain good agreement between data and predictions for the position of the solid–liquid interface. Bathelt *et al.* [4] conducted experiments on the heat transfer during the melting of paraffin from an array of three staggered cylinders. Much like in ref. [3] these authors concluded that natural convection effects should not be neglected in the analysis and design of systems involving latent heat of fusion energy storage. The results in refs. [3, 4] were extended by Bathelt and Viskanta [5] to the melting and solidification of paraffin around a finned heat source or sink. While the results in refs. [3–5] are thorough, they cannot be 'extrapolated' to the case of solidification of water. The reason for this fact is the presence of the density extremum of water in the vicinity of 4°C. This density extremum drastically affects the natural convection of water near the solidification interface [6, 7]. Hermann *et al.* [8] conducted experiments on the freezing of water around an isothermal horizontal cylinder surrounded by a concentrical cylindrical shell. They reported results on the growth of the ice–water interface and the temperature variation of the cylinder surface with time. Their study is of limited scope and does not determine or visualize the temperature field in the liquid phase. More importantly, the temperature gradients at the solidifying interface were not determined. These gradients are of paramount importance for the calculation of heat transfer rates at the solidification interface and therefore for the prediction of the progress of the solidification phenomenon.

Cheng *et al.* [9] investigated the effect of natural convection on ice formation around an isothermal horizontal pipe. Their experiments considered steady state conditions and they reported, most notably, results on the behavior of the average Nusselt number at the solidification interface as a function of the ambient temperature, the Rayleigh number and a modified Grashof number. Numerical and experimental results on steady state natural convection from a melting

NOMENCLATURE

b	fringe thickness at ice interface [m]
C_p	specific heat [J kg^{-1} K^{-1}]
d	pipe diameter [m]
k	thermal conductivity [W m^{-1} K^{-1}]
L	latent heat of solidification [J kg^{-1}]
N	fringe order number
n_1	refractive index of water at the interface (0 C)
n_2	refractive index of water one fringe from the interface
Nu	Nusselt number
P	pressure [bar]
s	direction perpendicular to the interface
Ste	Stefan number, $C_p(T_i - T_{w120})/L$
T	temperature [C]
T_i	temperature at the ice–water interface (0 C)
T_w	pipe wall temperature [C]
T_∞	reference (room) temperature (25 C)
t	time [s]
V^*	ratio of ice volume to total water chamber volume
W	enclosure length [m].

Greek symbols

ε	percent representative error
λ	wavelength of laser used
θ	position angle about the pipe.

Subscripts

1	ice–water interface
2	one fringe away from the interface
120	time of 120 min
i	interface
w	pipe wall
∞	reference (room) condition.

horizontal ice cylinder with emphasis on the stagnation point Nusselt number were published by Saitoh [10]. Shamsundar [11] and Sparrow and Hsu [12] reported theoretical predictions for the freezing of a liquid on the outside of a pipe carrying a coolant the temperature of which changes as it moves along the pipe. In both studies, the buoyancy driven flow outside the pipe was not taken into account. Gilpin [13] investigated the freezing of water inside a horizontal cylindrical pipe. He predicted theoretically the existence of three quasi-steady modes of convection for some temperatures in the vicinity of 4 C. He observed experimentally reversals of the flow pattern attributed to the existence of the density extremum. Dendritic ice formation was reported by Gilpin [14] during the freezing of supercooled water in a cylindrical pipe.

The present transient study significantly extends the body of existing knowledge on solidification of water around cold horizontal pipes [8–10]. Using holographic interferometry the local temperature gradients at the solidifying interface around a horizontal internally cooled pipe immersed in a rectangular water tank are carefully determined. In addition, visualization of the temperature field reveals interesting flow configurations existing in the liquid phase during the cooling process. Results on the pipe surface temperature dependence on time, the production of ice and the shape of the solidifying interface are also obtained in the course of the study.

2. EXPERIMENTAL SETUP AND TEST SECTION

All the temperature measurements in the liquid phase of the solidying water were performed using holographic interferometry. The experimental setup and the test section are discussed next.

The test section itself is basically a rectangular enclosure that is divided into three chambers; the central water chamber and two outer vacuum chambers as shown in Fig. 1. A photograph of the complete test section is shown in Fig. 2. The two side walls of the enclosure are made from $1\frac{1}{4}$ in. (3.175 cm) thick clear acrylic pieces and the top and bottom of the enclosure are made from 1 in. (2.54 cm) thick clear acrylic pieces. Note that one of the advantages of using holographic interferometry instead of Mach–Zehnder interferometry, is that with the former technique Plexiglas, which is easily machined and inexpensive, can be used to construct the test section. On the other hand, Mach–Zehnder interferometry requires the use of optic quality glass which is more expensive and not as easy to machine. The bottom and top pieces each have a drilled and tapped hole in the center for filling and overflow purposes. One of the side walls has all the necessary holes in it for the vacuum access to the outer chambers, the coolant pipe entrance and exit in the outer chambers, and the thermocouple leads in the central chamber. The dimensions of the inner water chamber are 4×4 in. (10.16 cm $\times$ 10.16 cm) square and 2 in. (5.08 cm) long. The two outer chambers have the same dimensions as the inner chamber except that they are only 1 in. (2.54 cm) long.

The four windows of the enclosure are made from $\frac{1}{2}$ in. (1.27 cm) thick clear acrylic pieces. The two outermost windows are simple windows attached to the side walls by eight # 10–24 socket head bolts and cemented air tight with silicon cement. The two inner windows separate the water chamber from the two

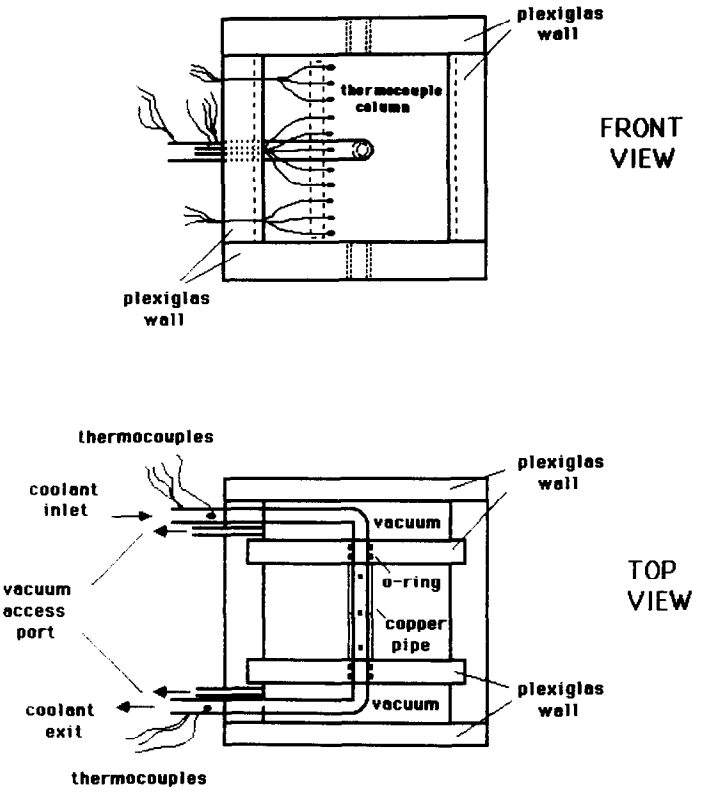

FIG. 1. Schematic of the experimental test section: front view and top view.

vacuum chambers and must have a hole in the center of each window to allow for the coolant pipe. The hole in the center of these two windows is slightly larger than $\frac{1}{4}$ in. (0.635 cm) in diameter and each window has two slots cut inside the central hole to fit two O-rings which seal the hole from leaking between the water and vacuum chambers.

The $\frac{1}{4}$ in. (0.635 cm) copper tubing coolant pipe enters the enclosure through one of the vacuum chamber's side walls, has a 90° elbow in the vacuum chamber, passes straight through the water chamber, has another 90° elbow after entering the other vacuum chamber, and exits through the side wall of the vacuum chamber (Figs. 1 and 2). In the water chamber the pipe diameter is increased by the addition of a copper sleeve to the total diameter of $\frac{3}{8}$ in. (0.9525 cm). This is done so that the O-rings used to seal the pipe at the windows do not obstruct the view of the pipe surface.

The fact that the coolant pipe enters and exits the vacuum chambers with the help of two 90° elbows was a refinement of the original design of the test section in which the copper pipe passed straight through the vacuum chambers and the test section. When the original design was tested, condensation problems were encountered on the front and rear outer walls of the apparatus where the pipe met the test section. Since holography was to be performed through these walls the condensation problems, even though not serious, were unacceptable. Therefore, the coolant pipe configuration was altered to that described above. Note that in the final design the coolant pipe exists through one of the side walls of the apparatus. Even if slight condensation occurs on the outer surface of this wall in the vicinity of the pipe, it has no effect whatsoever on the holography measurements which are performed through the front and rear walls.

There are six copper–constantan type thermocouples embedded in the coolant pipe section that is in the water chamber. The thermocouples are embedded in such a way that the bead of each thermocouple is at the outer surface of the copper tubing sleeve and the wire leads travel through the inside of the pipe until they exit the enclosure. Four of these thermocouples are located at the center of the water chamber at 90° intervals. The remaining two are at opposite ends of the water chamber and are embedded in the bottom of the sleeve. These six thermocouples are used to measure the surface temperature of the pipe in the water chamber. There are also two thermocouples outside the enclosure which are embedded in the pipe in such a way that the bed of the thermocouple is immersed in the coolant flowing through the pipe and they are used to measure the coolant temperature before it enters and after it leaves the enclosure. Ten additional thermocouples are attached to a transparent metric scale at 1 cm intervals located in the middle of the enclosure about 2 cm away from the pipe surface. This thermocouple column was used

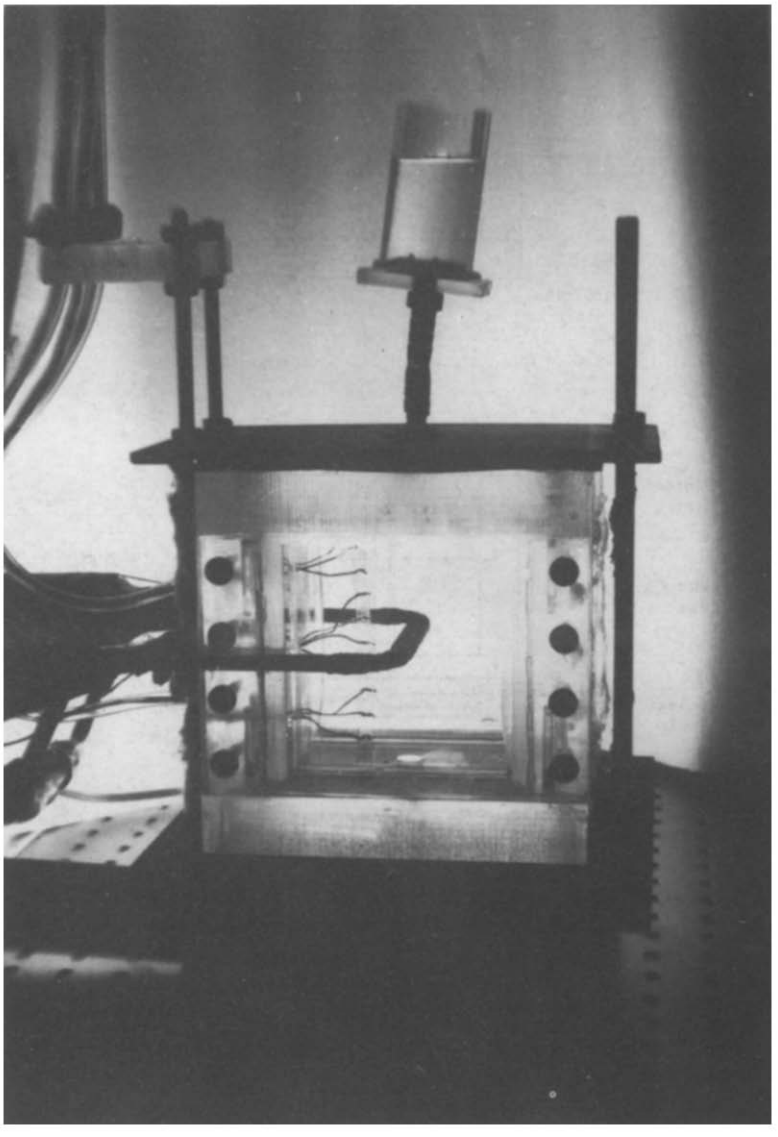

FIG. 2. Photograph of the test section.

primarily for focusing on the center of the enclosure and for scaling of the photographs. Also, during initial test runs the temperature measurements from the thermocouples were checked against the temperature measurements obtained via holographic interferometry.

A Hewlett Packard data acquisition and personal computer system was used to record all thermocouple readings, usually at 1 min intervals. The coolant flowing through the pipe is a mixture of 50% ethylene glycol and 50% distilled water. It was cooled and pumped through the pipe by a Brinkman RC20 recirculating bath refrigerator.

The optical equipment used to perform the experiments will be discussed next. The experiments were performed atop a 4×6 ft. (122 cm $\times$ 183 cm) optical table which was supported by compressed dry nitrogen. A schematic of the optical setup is shown in Fig. 3(a). The laser used was a 5 mW self-contained He–Ne laser. The beam was separated into the reference and object beams by a 5 mm cube type beam splitter. Each beam (reference and object) had its own spatial filter and collimator assembly. The design shown in Fig. 3(a) was used because the spatial filter and collimator are the last optical components before the beams impinged on the holographic plate. This yielded a clean plane wave for the reference and reconstruction beams. The focusing optics for the spatial filters where 4 mm focal length lenses and the pinholes were 12 μm in diameter. The collimators were 227.2 mm focal length three-element collimators with a maximum beam diameter of 50 mm. A simple ground glass diffuser was placed in the path of the object beam to scatter the light just prior to passing through the enclosure.

The plates used for these experiments were Agfa–Gevaert 10E75 holographic plates. The exposure time was determined by trial and error and for these holo-

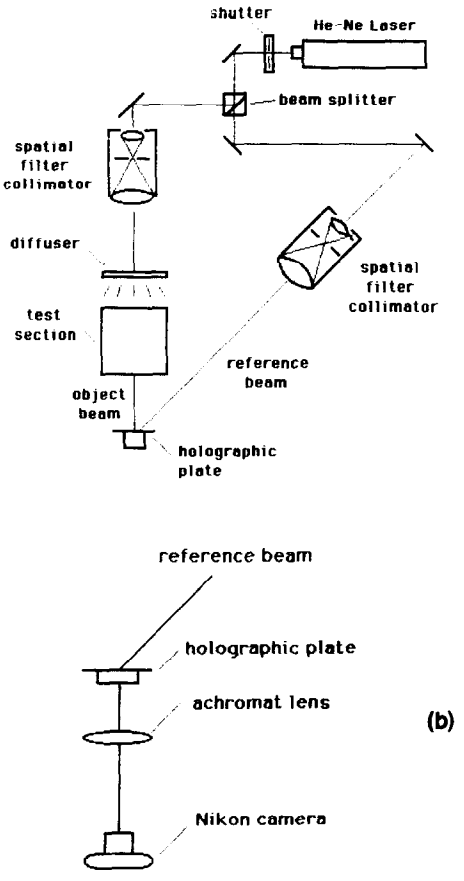

FIG. 3. (a) Experimental setup for the fabrication of the holograms. (b) Setup for the reconstruction and the photographic recording of the holograms.

graphic plates and optics configuration the exposure time was about $\frac{1}{10}$ s per exposure.

3. PROCEDURE

The test procedure begins with the alignment of the optics equipment, such as the spatial filters and collimators. Next, the circulating bath is cooled down to the desired operating temperature. The laboratory must be made light-tight prior to running the experiment since the laboratory acts, basically, like the inside of a camera.

After the lights are off, one holographic plate is removed from its light-tight box in a changing bag as an added precaution. The emulsion side of the holograms is determined by the moist finger technique. The side of the holographic plate that does not feel like clean glass is the emulsion side. The plate is placed in the holographic plate holder with the emulsion side facing the test section. At this point, the optics table is ready and is not touched until the experiment is finished.

The data acquisition system is started next and after a few minutes of recording all the thermocouple readings at reference state (room temperature) the first exposure of the hologram is taken. Immediately following the first exposure the valve to the recirculating bath is opened and the coolant starts flowing through the pipe. The data acquisition system scans the thermocouples every minute and is used as a timer so that after a prescribed number of scans (75, 90, 105 and 120) the second exposure is taken. The hologram is then removed from the plate holder, placed in a light-tight container, and taken to the darkroom for developing.

The developing procedure for the hologram is a combination of the procedure given by Vest [15] and the procedure given by Lizuka [16] with the bleaching formula by Jeong [17]. The sequence of steps in the developing procedure is reported next for completeness. They are intended to aid the reader to construct holograms of the type obtained in this study, without going through a tedious trial and error process. The above-mentioned steps are as follows: (1) develop in D-19 for 5 min; (2) bathe in indicator stop bath for 30 s; (3) immerse in fixer for 6 min; (4) rinse with water for 30 s; (5) clean with Hypo cleaning agent for 2 min; (6) rinse with water for 10–30 min; (7) bleach until transparent; (8) rinse with water for 5 min; (9) immerse in photoflo for 30 s; (10) hang until dry. Bleaching of the holographic plate converts the hologram from an intensity hologram to a phase hologram which is much brighter and easier to photograph when reconstructed. The wet bleaching technique used here was simply the submergence, with agitation, of the plate in a solution of potassium dichromate, sulfuric acid, and water. As in the developing of any film, agitation is required for every step of the developing procedure.

The developed holographic plate was placed in the plate holder in its original position and illuminated with the reconstruction beam, which was the same as the reference beam during the exposures (Fig. 3(b)). The object beam was blocked and the virtual image was photographed with a 35 mm camera using T-max 100 film. This film was developed and large prints were made of each hologram. An angular grid was drawn on the prints at 5° intervals and these prints were photographed again. This second photograph was taken using Polagraphic HC film and yielded slides where the print was magnified such that only about 30° of the ice–water interface would fit on one slide. The slides were put on an optical comparator and the final image on the comparator screen was about 150 × magnification of the original object. The fringe thickness at the ice–water interface was measured and used for the evaluation of the local Nusselt number.

The local Nusselt number at any point around the solidifying interface was defined as

$$Nu = \frac{\left[k\left(\frac{\mathrm{d}T}{\mathrm{d}s}\right)_i\right]d}{(T_s - T_i)k} \qquad (1)$$

where all the symbols in the above and the subsequent equations are defined in the Nomenclature. The temperature gradient at the interface is approximated by the temperature change across the fringe at the interface (ΔT) divided by the thickness of that fringe (b), i.e.

$$\left(\frac{\mathrm{d}T}{\mathrm{d}s}\right)_i \approx \frac{\Delta T}{b}. \tag{2}$$

Combining equations (1) and (2) yields

$$Nu \approx \frac{\Delta T}{b}\frac{d}{T_\infty - T_i}. \tag{3}$$

Taking into account that 'b', the fringe thickness, can be obtained from the reconstructed hologram, the only quantity yet unknown in the above equation is ΔT, the temperature change across the fringe thickness. Note that the temperature at the interface is known namely 0°C (the freezing temperature of pure water). Therefore, only the temperature at the other edge of the fringe needs to be determined. To achieve this goal, first we use the fact that the phase shift of the reconstructed virtual image is given by [15]

$$N\lambda = (n_1 - n_2)W \tag{4}$$

where N is the fringe order, λ the wavelength of the laser light, W the length of the water chamber of the test section and n the index of refraction. Subscripts 1 and 2 refer to two locations on the hologram. In the present study since we are interested in the change of the index of refraction across the fringe at the solidifying interface subscripts 1 and 2 correspond to the two edges of that fringe and $N = 1$.

The index of refraction is, in general, a function of wavelength, temperature and pressure. Correlations for the index of refraction are reviewed in Thormahlen *et al.* [18]. One of the correlations these authors presented for the index of refraction of water obtained using the Lorentz–Lorenz equation did not perform well when checked against our data in the neighborhood of the density extremum of water at 4°C. The most popular equation for the refractive index of water is that given by Tilton and Taylor [19]. The refractive index correlation used in the present study was that proposed by Thormahlen *et al.* [20] which very closely matches the Tilton and Taylor relationship, however, it is more exact and has a wider range of validity. According to ref. [20] the index of refraction of water is given by

$$\begin{aligned} n(\lambda, T, P) = {} & \sqrt{\left(\frac{a_1}{\lambda^2 - \lambda_{\mathrm{uv}}^2} + a_2 + a_3\lambda^2 + a_4\lambda^4 + a_5\lambda^6\right)} \\ & + (b_1 + b_2\lambda^2 + b_3\lambda^4)(T - T_\mathrm{b}) + (b_4 + b_5\lambda^2 \\ & + b_6\lambda^4)(T - T_\mathrm{b})^2 + (b_7 + b_8\lambda^2 + b_9\lambda^4)(T - T_\mathrm{b})^3 \\ & + [c_1 + c_2\lambda^2 + (c_3 + c_4\lambda^2)T](P - P_\mathrm{b}) \\ & + (c_5 + c_6\lambda^2)(P - P_\mathrm{b})^2. \end{aligned} \tag{5}$$

The range of validity for equation (5) is 0.182 μm $\leq \lambda \leq$ 2.770 μm, -10°C $\leq T <$ 100°C, 1 bar $\leq P <$ 1200 bar. The values of all the constants and parameters in equation (5) are reported in the Appendix. The parametric domain of our study is, clearly, well within the range of validity of equation (5).

The index of refraction (n_1) at the edge of the fringe that coincides with the solidifying interface was obtained directly from equation (5) since, as discussed earlier the temperature is known at this location ($T = 0$°C). With n_1 known, the index of refraction at the other edge of the fringe (n_2) can be calculated from equation (4). Next, with n_2 known, equation (5) yields the temperature at the edge of the fringe corresponding to n_2. Based on the above discussion, the temperatures at both edges of the fringe at the solidifying interface are determined so that ΔT and, subsequently, Nu can be calculated from equation (3). This procedure for evaluating Nu needs to be repeated at every angular location around the phase change front.

Before closing this section it is necessary to define and discuss the errors associated with the measurement of the local Nusselt number. Two major contributions to a representative error (ε) are identified: the error associated with measuring the fringe thickness and the error associated with diffraction effects. The measurement error is inversely proportional to the fringe thickness. In our study this error was reduced by magnifying the image and by using an accurate measuring device as explained earlier. The diffraction error is due to the fact that the solidifying interface acts as a surface. This error is inversely proportional to the square of the fringe thickness. The change in the fringe order caused by the diffraction error is given by Hauf and Grigull [21]

$$\Delta N = \frac{n_\infty \lambda L}{12 b^2}. \tag{6}$$

Note that T_∞ has no effect on the accuracy of the results for Nu. It was not used in equations (4) and (5) for the evaluation of the temperature gradients. The ice–water interface temperature which is known exactly (0°C) was used as the 'known' temperature in the evaluation of the temperature gradients. The quantity T_∞ (room temperature) is a known constant (25°C) used for non-dimensionalization purposes only in equations (1) and (3). The representative error, the sum of the two errors mentioned above, for a typical case in our study is shown in Fig. 4. It reaches a maximum of about 8% in the vicinity of $\theta = 270°$ where the fringes are the thinnest and they are spaced the closest. For $\theta < 180°$ the representative error remains less than 2%. In summary, it is felt that the error involved in our measurements for Nu is relatively small, which is aided by the fact that the interface temperature is known (0°C). Uncertainties as large as 15% in the measurement of Nu using holographic interferometry have been reported in the literature [22].

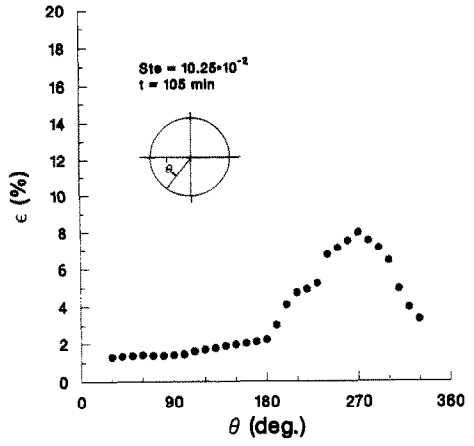

FIG. 4. Representative total error (ε) in the measurements for Nu.

4. RESULTS AND DISCUSSION

The discussion of the results starts with the variation of the pipe wall temperature with time. Note that all the thermocouples installed on the pipe wall in the manner discussed in the previous section register the same temperature within 0.2°C. The wall temperature reported is the arithmetic mean of all temperatures recorded. For all three values of the Stefan number examined, the wall temperature exhibits a drastic decrease at early times, when the coolant starts circulating through the pipe (Fig. 5). The rate of decrease levels off thereafter. The time at which ice first forms on the outer surface of the pipe is identified by a 'jump' on the temperature history curves. This jump is caused by the latent heat of fusion released at the surface of the pipe when ice first forms as well as the fact that the interface is at 0°C. Thereafter, the temperature of the pipe surface keeps decreasing but at a much slower rate, until at late times the rate of decrease is small enough so that the temperature of the pipe reaches, for all practical purposes, a plateau. To exemplify, based on the data in Fig. 5, the rate of decrease of the pipe wall temperature for $Ste = 6.20 \times 10^{-2}$ is 20.9°C min^{-1} at $t = 1$ min,

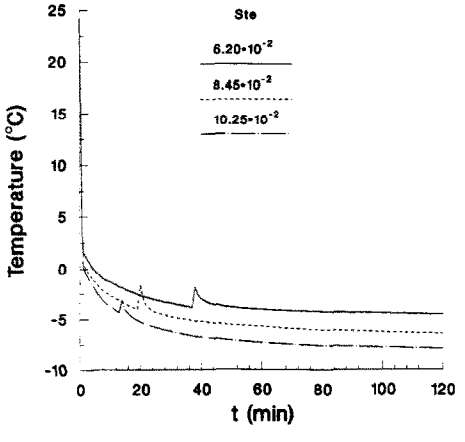

FIG. 5. The variation of the pipe wall temperature with time.

7.49×10^{-2}°C min^{-1} at $t = 30$ min and 1.12×10^{-2} °C min^{-1} at $t = 100$ min. Note that the temperature T_{w120} used in the definition of Ste throughout this study (see the Nomenclature) is the value of the wall temperature at $t = 120$ min at which time the wall temperature is practically constant.

Because of the presence of convection in the liquid phase prior to solidification, ice starts to form on the pipe surface after the temperature of the surface is below the freezing temperature of water. The ice formation temperature decreases and the ice formation time decreases as the value of Ste increases.

An interesting result is revealed by the visualization of the temperature field at early times and it is shown in Fig. 6. A strong natural convection plume is formed on the under side of the pipe at early times. This plume is not symmetric and it swings from left (Fig. 6(a)) to right (Fig. 6(b)). Note that as the plume swings, it 'splits' into a 'primary' and a 'secondary' branch. The secondary branch is visible under the primary branch in Figs. 5(a) and (b). At later times, as the temperature differences in the cavity decrease through convective mixing as well as conduction in the liquid phase, the flow is milder and the plume actually disappears (Figs. 7(a) and (b)). Of interest also is the shape of the ice body that has formed around the pipe (Figs. 7(a) and (b)). The ice thickness is much larger under the pipe than it is on top of the pipe. The reason for this asymmetry in the shape of the ice layer is the buoyancy driven flow which moves fast parallel to the ice surface situated on the upper portion of the pipe thus retarding the ice formation. More specifically, note that the approximate location of the 4°C isotherm was estimated to be about three fringes away from the interface in Fig. 7. Since the density extremum of water occurs at 4°C, its presence aids the flow in the upper part of the interface and retards the flow in the lower part.

It is worth clarifying that the fringe thickness near the interface in Fig. 6 cannot be read accurately to provide reliable measurements for Nu. Figure 6 corresponds to rather 'early' times at which the temperature gradients near the interface are very steep and result in high fringe densities. All the measurements for Nu in this paper are for later times at which the fringe thickness at the interface can be read clearly as exemplified by Fig. 7. Figure 6 was used only for the 'visualization' of the temperature field and not for actual data reduction. In addition, freezing has not begun in the photograph of Fig. 6(b). This is why some fringes are visible all the way to the cylinder surface.

Detailed results on the shape of the solidifying interface are reported in Figs. 8 and 9. These figures were produced by tracing photographs. For all values of Ste, as time increases, the thickness of the ice layer increases at all points around the pipe. For a fixed time, increasing Ste yields a thicker ice layer (Fig. 9). The ice layer is not always approximately symmetric about the vertical axis of symmetry of the pipe. Note,

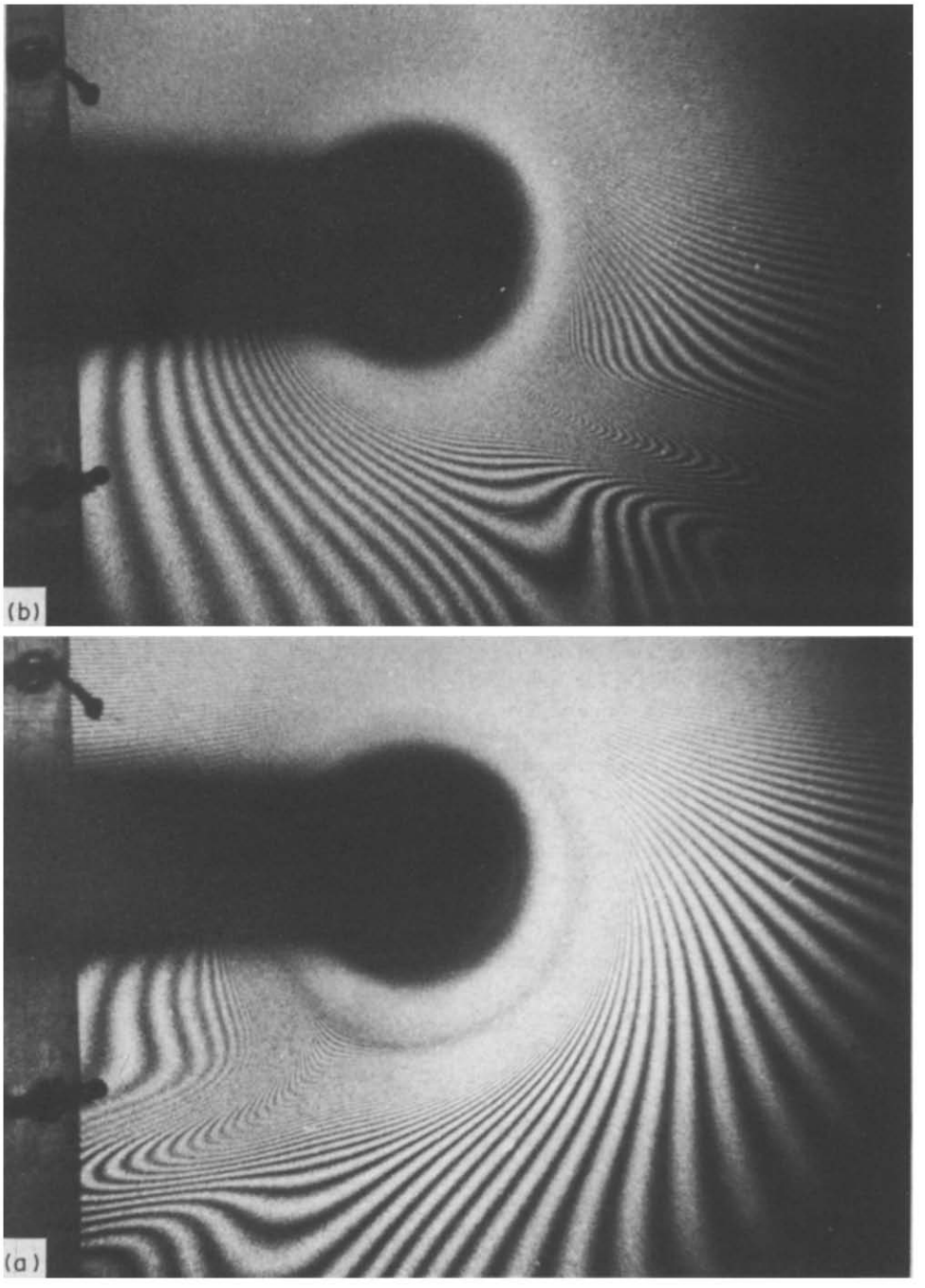

FIG. 6. Representative photographs of holograms at later times, after ice is formed around the pipe: (a) $t = 30$ min, $Ste = 8.45 \times 10^{-2}$; (b) $t = 20$ min, $Ste = 8.45 \times 10^{-2}$.

for example, the shape of the solidifying interface for $Ste = 8.45 \times 10^{-2}$ at $t = 20$ and 40 min as well as for $Ste = 10.25 \times 10^{-2}$ at $t = 20$ and 40 min (Fig. 8). The reason for this asymmetry is the unstable nature of the plume existing at the early stages of the solidification. The asymmetry in the thickness of the ice layer 'swings' as the plume swings. At later times, when the plume practically disappears, the ice–water interface becomes gradually symmetric about the vertical axis of symmetry.

Figure 10 illustrates the variation of the ice volume produced around the pipe as a function of time. For all three values of *Ste* examined, the volume of ice produced increases linearly, for all practical purposes, with time. The higher the value of *Ste* the larger the amount of ice produced at any specific time. In addition, the rate of ice production ($dV^*/d\tau$) increases as the value of the Stefan number increases.

A major goal of this study was to obtain measurements of the local Nusselt number around the solidifying interface using holographic interferometry. Such measurements are reported in Fig.

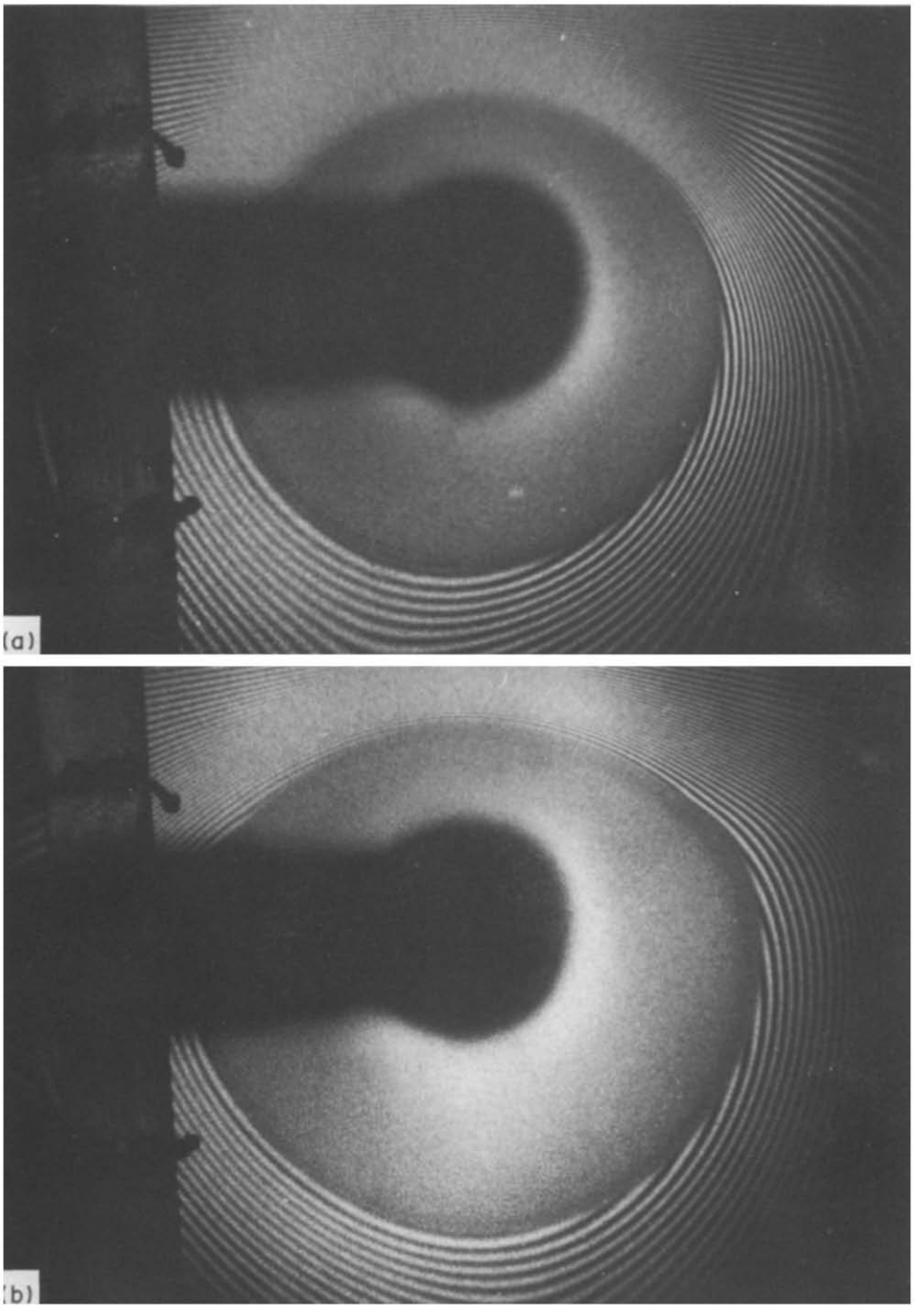

FIG. 7. Representative photographs of holograms at later times, after ice is formed around the pipe: (a) $t = 90$ min, $Ste = 8.45 \times 10^{-2}$; (b) $t = 120$ min, $Ste = 8.45 \times 10^{-2}$.

11 for $Ste = 6.20 \times 10^{-2}$. The local Nusselt number increases as θ increases, reaches a maximum at $\theta \approx 270°$ and thereafter decreases. Overall, the Nusselt number variation with θ resembles a bell-shaped curve at all times. The fact that the heat transfer maximum occurs in the vicinity of $\theta \approx 270°$ is explained by the visualization of the temperature field discussed earlier (Fig. 7): the sharp thermal boundary layer existing on the top portion of the pipe (and in particular in the vicinity of $\theta = 270°$) weakens gradually as we move toward the bottom half of the pipe where, as the holograms indicate, the temperature gradients at the interface are not as steep. As the time increases from $t = 80$ to 120 min the local Nusselt number generally decreases, even though the dependence of Nu on θ remains qualitatively the same.

Figure 12 presents data similar to those of Fig. 11 but for a higher Stefan number ($Ste = 8.45 \times 10^{-2}$). The dependence of Nu on position (θ) remains qualitatively the same to that discussed earlier in con-

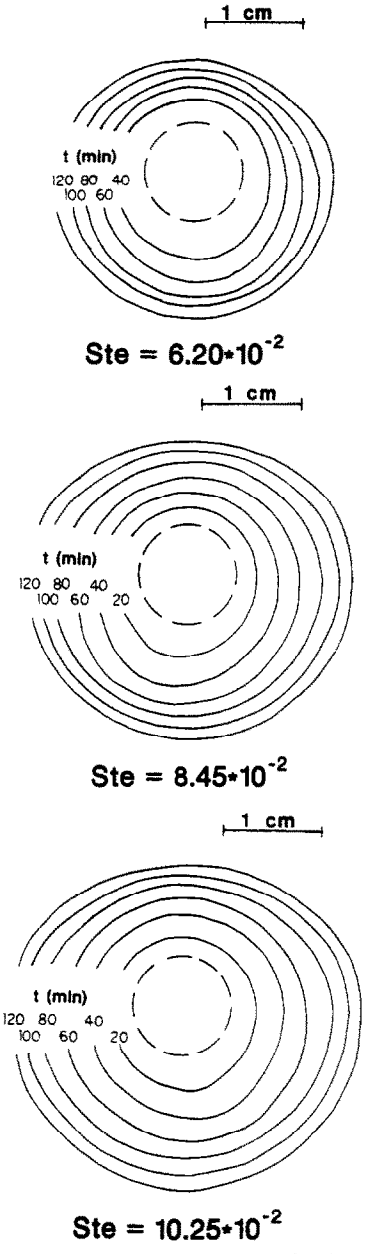

FIG. 8. The advancement of the solidification interface in time for representative values of the Stefan number.

nection with Fig. 11. The values of *Nu* appear to generally decrease if *Ste* increases and the remaining parameters remain unchanged. This fact is illustrated in Fig. 13 where the variation of *Nu* with θ for three values of *Ste* and for $t = 90$ min is presented. To explain the dependence of *Nu* on *Ste* first recall that increasing *Ste* is equivalent to decreasing the late time wall temperature based on which the Stefan number is defined. Second, all the results in Figs. 11–13 for the local Nusselt number are for rather late times, well after the time at which ice first forms. It appears that the buoyancy driven flow at late times is weaker for larger values of *Ste*. The opposite is expected to be true at early times, in particular before ice is formed, since

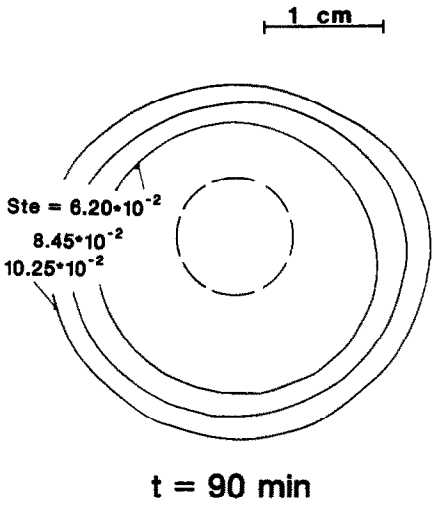

FIG. 9. The effect of *Ste* on the solidification interface for $t = 90$ min.

large values of *Ste* correspond to lower wall temperatures and, therefore, higher *initial* temperature differences between the pipe wall and the water in the system. It is reasonable then to claim that the cooling effect of the pipe 'propagates' faster in the enclosure (through water circulation and mixing) for larger values of *Ste*. As a result, at later times, well after the ice is formed, the temperature differences existing in the liquid driving the natural convection are likely to be smaller for larger values of *Ste*. This explains the fact that, overall, at late times incresing *Ste* decreases the local Nusselt number. Taking into account the complexity of the transient phenomenon of interest it should be noted that the above reasoning is meant to serve only as a guide to explain the trend of the results in Fig. 13.

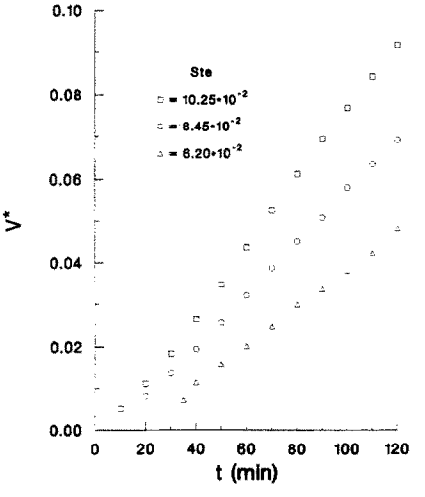

FIG. 10. The time history of the ice production.

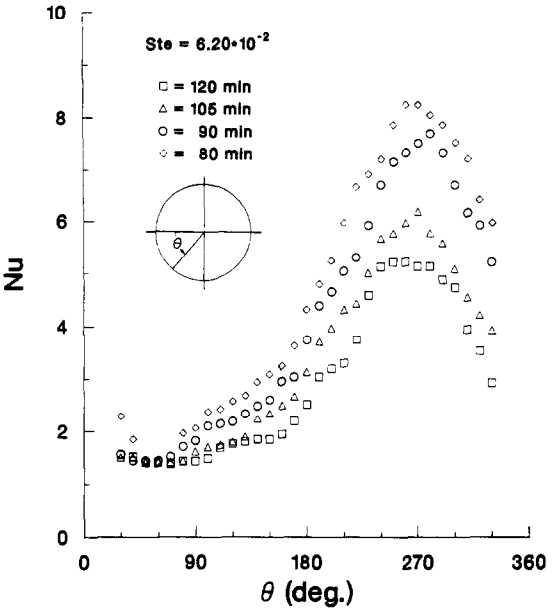

FIG. 11. The local Nusselt number at the solidifying interface for $Ste = 6.20 \times 10^{-2}$.

5. CONCLUSIONS

In this paper, the main results of an experimental study on the transient freezing of water around a horizontal pipe were reported. Holographic interferometry was used to visualize the temperature field in the liquid phase and to determine the local Nusselt number at the solidifying interface. It was found that an unstable plume swinging from left to right and moving downward exists during the early stages of solidification phenomenon. This plume causes the shape of the solidification interface to be asymmetric about the vertical axis passing through the center of the pipe. At later times, as the temperature differences in the liquid phase diminish through mixing resulting from the water circulation, the plume weakens and practically disappears. As a result symmetry about the vertical axis is, approximately, established. Because of the structure of the flow in the system, the thickness of the ice layer is the smallest in the upper portion of the pipe.

The pipe surface temperature decreases rapidly at first, experiences a sudden discontinuity (rise) when ice is formed and keeps decreasing slowly thereafter

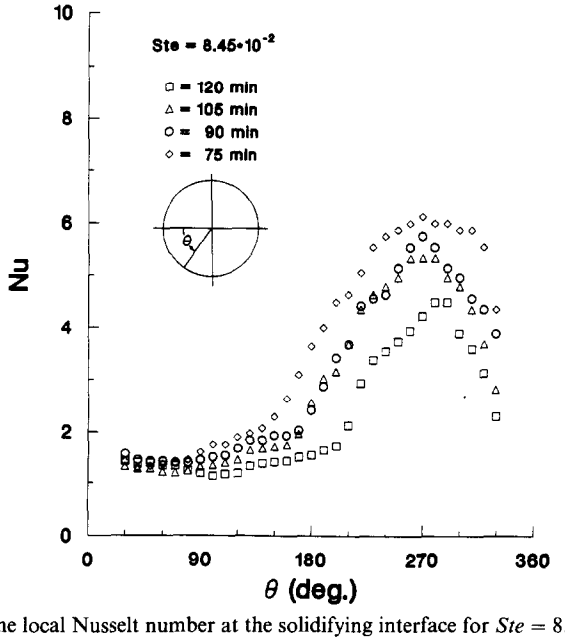

FIG. 12. The local Nusselt number at the solidifying interface for $Ste = 8.45 \times 10^{-2}$.

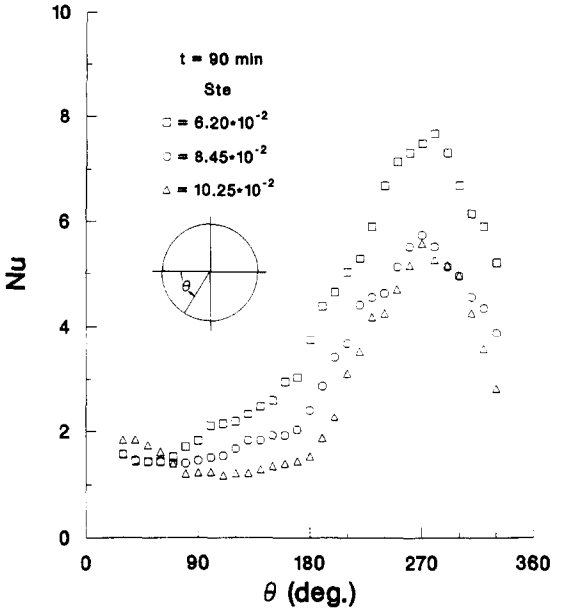

FIG. 13. The effect of *Ste* on the local Nusselt number at the interface for $t = 90$ min.

until, at later times, it becomes practically constant. The ice volume production increases almost linearly with time.

The local Nusselt number variation around the solidifying interface is non-monotonic. Nusselt number increases starting from $\theta \approx 90°$, reach a maximum at $\theta \approx 270°$ and decrease thereafter. This behavior of *Nu* was consistent for all times and values of *Ste* examined. The effect of increasing *Ste at late times* was to, generally, decrease the value of *Nu*.

Taking into account the fact that temperature measurements in the liquid phase of solidifying water and in particular measurements of the local Nusselt number at the solidifying interface are indeed rare in the literature, the results presented in this paper can also be used to verify numerical simulations on the transient solidification of water.

Acknowledgement—This work was supported by the National Science Foundation through grant No. ENG 84-51144.

REFERENCES

1. J. Reimann, Experimental investigation of free convection flow from wires in the vicinity of phase interfaces, *Int. J. Heat Mass Transfer* **17**, 1051–1060 (1974).
2. G. Antonini, G. Guiffant and P. Perrot, The effect of transverse oscillations on heat transfer from a horizontal hot-wire to a liquid, holographic visualization, *Int. J. Heat Mass Transfer* **20**, 88–92 (1977).
3. A. G. Bathelt, P. D. Van Buren and R. Viskanta, Heat transfer during solidification around a cooled horizontal cylinder, *A.I.Ch.E. Symp. Ser. No.* 189 **75**, 103–111 (1979).
4. A. G. Bathelt, R. Viskanta and W. Leidenfrost, Latent heat-of-fusion energy storage: experiments on heat transfer from cylinders during melting, *J. Heat Transfer* **101**, 453–458 (1979).
5. A. G. Bathelt and R. Viskanta, Heat transfer and interface motion during melting and solidification around a finned heat source/sink, *J. Heat Transfer* **103**, 720–726 (1981).
6. T. L. Spatz, D. Poulikakos and M. Kazmierczak, High Rayleigh number experiments in a horizontal layer of cold water, *J. Heat Transfer* **111**, 578–581 (1989).
7. M. Kazmierczak and D. Poulikakos, Melting of an ice surface in porous medium, *AIAA J. Thermophys. Heat Transfer* **2**, 352–358 (1988).
8. J. Hermann, W. Leidenfrost and R. Viskanta, Effect of natural convection on freezing of water around an isothermal, horizontal cylinder, *Int. Commun. Heat Mass Transfer* **11**, 301–310 (1984).
9. K. C. Cheng, H. Inada and R. R. Gilpin, Effects of natural convection on ice formation around an isothermally cooled horizontal cylinder, *J. Heat Transfer* **110**, 931–937 (1988).
10. T. Saitoh, Natural convection heat transfer from a horizontal ice cylinder, *Appl. Scient. Res.* **32**, 429–451 (1976).
11. N. Shamsundar, Formulae for freezing outside a circular tube with axial variation of coolant temperature, *Int. J. Heat Mass Transfer* **25**, 1614–1616 (1982).
12. E. M. Sparrow and C. F. Hsu, Analysis of two-dimensional freezing on the outside of a coolant-carrying tube, *Int. J. Heat Mass Transfer* **24**, 1345–1357 (1981).
13. R. R. Gilpin, Cooling of a horizontal cylinder of water through its maximum density point at 4°C, *Int. J. Heat Mass Transfer* **18**, 1307–1315 (1975).
14. R. R. Gilpin, The effects of dendritic ice formulation in water pipe, *Int. J. Heat Mass Transfer* **20**, 693–699 (1977).
15. C. M. Vest, *Holographic Interferometry*. Wiley, New York (1979).
16. K. Lizuka, *Engineering Optics*, Springer Series in Optical Sciences, Vol. 35. Springer, Berlin (1987).
17. T. H. Jeong, Private communications, Lake Forest College, Illinois (1989).
18. J. Thormahlen, J. Straub and U. Grigull, Refractive index of water and its dependence on wavelength, temperature, and density, *J. Phys. Chem. Ref. Data* **14**, 933–945 (1985).

19. L. W. Tilton and J. K. Taylor, Refractive index of distilled water for visible radiation at temperature 0°C to 60°C, *J. Res. Natn. Bur. Stand.* **20,** 419 (1938).
20. I. Thormahlen, K. Scheffler and J. Straub, Water and steam, *Proc. 9th ICPS*, p. 477. Pergamon Press, Oxford (1980).
21. W. Hauf and U. Grigull, Optical methods in heat transfer, *Adv. Heat Transfer* **6,** 133–367 (1970).
22. Y. Gogus, Investigation of laminar natural convection heat transfer around an isothermal U-shaped body. In *Natural Convection: Fundamentals and Applications*. NATO, Scientific Affairs Div., Brussels, Belgium (1985).

APPENDIX

Values of constants in equation (5)

$T_b = 20°C$

$P_b = 1.01325$ bar

$\lambda_a^2 = 0.018085\ \mu m^2$

$a_1 = 5.743534 \times 10^{-3}$

$a_2 = 1.769238$

$a_3 = -2.797222 \times 10^{-2}$

$a_4 = 8.715348 \times 10^{-3}$

$a_5 = -1.413942 \times 10^{-3}$

$b_1 = -8.454823 \times 10^{-5}$

$b_2 = -2.787742 \times 10^{-5}$

$b_3 = 2.608176 \times 10^{-6}$

$b_4 = -2.050671 \times 10^{-6}$

$b_5 = 1.019989 \times 10^{-6}$

$b_6 = -2.611919 \times 10^{-6}$

$b_7 = 8.194989 \times 10^{-9}$

$b_8 = -8.107707 \times 10^{-9}$

$b_9 = 4.877274 \times 10^{-8}$

$c_1 = 8.419632 \times 10^{-6}$

$c_2 = 1.941681 \times 10^{-5}$

$c_3 = -7.762524 \times 10^{-8}$

$c_4 = 4.371257 \times 10^{-8}$

$c_5 = 7.089664 \times 10^{-9}$

$c_6 = -2.240384 \times 10^{-8}$.

EXPERIENCES PAR INTERFEROMETRIE HOLOGRAPHIQUE SUR LA CROISSANCE DE LA GLACE A PARTIR D'UN TUBE HORIZONTAL

Résumé—On rapporte les résultats principaux d'une étude expérimentale sur la croissance de la glace à partir d'un tube horizontal intérieurement refroidi et immergé dans l'eau. A l'aide de l'interférométrie holographique, le nombre de Nusselt local à l'interface de solidification est obtenu à des temps caractéristiques pendant l'évolution du phénomène de solidification. La visualisation prouve que les champs de température et d'écoulement sont dissymétriques et instables aux premiers stades de la solidification. Un panache dû au flottement se développe sur la base du tube. Ce panache oscille continûment autour de l'axe vertical de symétrie et affecte le mécanisme de solidification. Des résultats supplémentaires concernent l'évolution de l'interface de changement de phase avec le temps, la dépendance de la température de la paroi du tube et du volume de glace produit vis-à-vis du temps.

UNTERSUCHUNG DES EISWACHSTUMS AN EINEM HORIZONTALEN ROHR MIT HILFE DER HOLOGRAPHISCHEN INTERFEROMETRIE

Zusammenfassung—In der vorliegenden Arbeit wird über die wichtigsten Ergebnisse einer experimentellen Untersuchung der Eisbildung an einem von innen gekühlten, außen von Wasser umgebenen horizontalen Rohr berichtet. Mit Hilfe der holographischen Interferometrie wird zu charakteristischen Zeiten während des Erstarrungsvorgangs die örtliche Nusselt-Zahl an der Erstarrungsfront ermittelt. Eine Sichtbarmachung hat gezeigt, daß Temperatur- und Strömungsfelder im frühen Stadium der Erstarrung asymmetrisch und instabil sind. An der Unterseite des Rohrs bildet sich aufgrund der Dichteunterschiede eine Strömungsfahne, die sich nach unten ausdehnt. Diese Strömungsfahne schwingt ständig um die vertikale Symmetrieachse des Systems und beeinflußt den Erstarrungsvorgang. Weitere Schlüsselergebnisse dieser Arbeit betreffen die zeitliche Entwicklung der Phasengrenze, der Temperatur der Rohrwand und des gebildeten Eisvolumens.

ЭКСПЕРИМЕНТАЛЬНОЕ ИССЛЕДОВАНИЕ РОСТА ЛЬДА НА ГОРИЗОНТАЛЬНОЙ ТРУБЕ С ИСПОЛЬЗОВАНИЕМ ГОЛОГРАФИЧЕСКОЙ ИНТЕРФЕРОМЕТРИИ

Аннотация—Представлены основные результаты экспериментального исследования роста льда на погруженной в воду горизонтальной трубе с внутренним охлаждением. С помощью голографической интерферометрии определено локальное число Нуссельта у границы раздела в процессе затвердевания. Визуализация показала, что поля температуры и течения на ранних стадиях затвердевания являются несимметричными и нестационарными. В трубе за счет подъемных сил образуется текущая вниз струя. Эта струя постоянно смещается относительно вертикальной оси симметрии и оказывает воздействие на процесс затвердевания. Кроме того, в статье приведены результаты по временной эволюции межфазной границы, а также по временной зависимости температуры стенки трубы и объема образующегося льда.